Grant Agreement No.: 604656

Project acronym: NanoSim

Project title: A Multiscale Simulation-Based Design Platform for Cost-Effective CO_2 Capture Processes using Nano-Structured Materials (NanoSim)

Funding scheme: Collaborative Project

Thematic Priority: NMP

THEME: [NMP.2013.1.4-1] Development of an integrated multi-scale modelling environment for nanomaterials and systems by design

Starting date of project: 1st of January, 2014

Duration: 48 months

Document ID: NanoSim-WP4-D4.5_Deliverable_CodeModulesReactiveHeatMassTransfer

WP N°	Del. N°	Title	Contributors	Version	Lead beneficiary	Nature	Dissemin. level	Delivery date from Annex I	Actual delivery date dd/mm/yyyy
4	D4.5	Models on Heat and Mass Transfer	Authors: Thomas Forgber, Federico Municchi, Stefan Radl Checked by: Stefan Radl	1.2	TUG	Other	PU	30/06/2016	20/07/2016

1 Introduction

This document summarizes the work done on heat and mass transfer (with and without reactions) using CFDEMcoupling, specifically in tasks 4.5 and 4.6 of the DoW. The focus was on the following work items:

- Collection of experimental data (for heat transfer, and hydrodynamics) in fixed and fluidized beds in order to collect data for a subsequent validation study.
- Demonstration of the code modules to be used for heterogeneous reactions in a non-isothermal gas-particle mixture (including ability to include sophisticated models that account for the fluctuation of the heat transfer coefficient).
- Reversibility testing of the code modules against Direct Numerical Simulations.
- Validation studies relying on particle-unresolved Euler-Lagrange simulations using CFDEM(R)coupling and the collected experimental data.

1.1 Document identification

Document Identification	CODEMODULES_REACTIVE_HEAT_MASS
Author(s)	Thomas Forgber, Federico Municchi, Stefan Radl
Reviewers	Stefan Radl
Manager	Stefan Radl (TUG)
Version of the Product	1.2
Version of “ParScale”	1.1.1.-beta
Version of “CPPPO”	1.0.1-beta
Version of “CFDEM”	3.4.0 (branch CFDEMcoupling-RADL/master)

1.2 Scope

Code modules were developed which enable the co-simulation platform to perform simulations involving heat and (reactive) mass transfer. Predictions are compared (to a certain complexity) to in-house experiments, as well as to analytical solutions. The experimental setup is based in a quasi two-dimensional (i.e., shallow) fluidized bed, which was further developed and extended by the ability to measure temperatures inside the bed of particles. Therefore, a heat exchanger was designed which is capable of heating the incoming compressed air. This provides different operating points of the particle bed (i.e., from the packed to the fluidized bed regime). From the experimental setup we are able to recover the overall heat transfer rate, the temperature distribution in the particle bed, as well as the local volume fraction and particle velocity distribution within the particle bed. Some of this data is compared to simulations relying on the fully coupled CFDEM-LIGGGHTS-ParScale package, i.e., the COSI platform.

1.3 References

Acronym	Name
DOW	Description of Work (Work Package 4)
OPH-PRIV	Online Project Hosting – Private (available to the consortium only)
OPH-PU	Online Project Hosting – https://github.com/CFDEMproject/CFDEMcoupling-PUBLIC for CPPPO)
CPPPO	Compilation of fluid/Particle Post Processing routines

1.4 System Overview

CFDEM®'s Immersed Boundary solver (see Deliverable 4.3) has been developed and applied to study flow and transport phenomena in dense particle beds.

CFDEM's unresolved EL solver (i.e., the classical "CFDEMcoupling") has been upgraded to couple the code simulations tools:

- ParScale (including CHEMKIN-II interface, as well as models to handle heterogeneous reactions)
- CPPPO (see Deliverable 4.1)

Both simulation tools have been already documented in Deliverable 4.1, and are integrated as shown in Figure 1. Most important, CFDEMcoupling was designed such that the coupling to ParScale can be de-activated, i.e., LIGGGHTS can be used to predict the outcome of simple reactions.

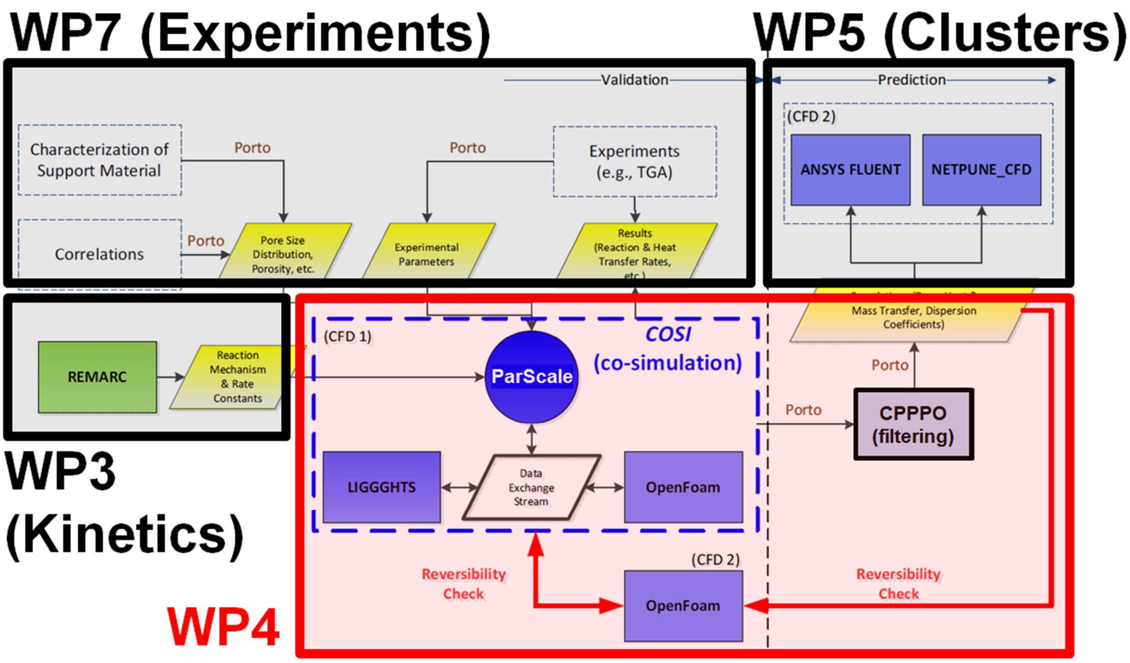

Figure 1. Overview of work packages interfacing with the tools "ParScale" and "CPPPO" developed in WP 4 (from report of Deliverable 4.1).

1.5 Overview of the Use Cases

In order to generate reliable date for the development of the heat and mass transfer model, a set of verification and validation cases has been defined (see Table 1).

Table 1: Overview of relevant verification and validation cases for the IB and PU-EL solver.

Use Case Name	Key Feature
1 - fluidizedBedTemp	fluidized bed with homogeneous particle temperature
2 - fluidizedBedTempParScale	fluidized bed with inhomogeneous particle temperature
3 - packedBedTemp	packed bed with homogeneous particle temperature
4 - packedBedTempParScale	packed bed with inhomogeneous particle temperature
5 - periodicArray_IB	Periodic array with inhomogeneous particle temperature & DNS immersed boundary solver
6 - periodicArray_EL	Periodic array with inhomogeneous particle temperature & unresolved Euler-Lagrange solver
7 – CHEMKIN-II test case	Github: ParScale/examples/testCases/chemistryReader_Andersson
8 - twoStageFB	Demonstration: case to demonstrate the usage of CFDEMcoupling without ParScale, i.e., LIGGGHTS will predict the outcome of a simple heterogeneous reaction occurring uniformly within a porous particle

1.6 Organization and Responsibilities

TUG was responsible for implementation, documentation, verification & validation, simulation and experimental work, while DCS contributed with respect to the code architecture, reviewing activities and test harness integration.

1.7 Applied Workflow

The following workflow was followed during the development process of the model:

- Implementation of coupling models in the "CFDEMcoupling" framework (mainly heat and mass transfer models), as well as LIGGGHTS (in order to hand over heat and mass fluxes to ParScale, as well as to robustly integrate particle quantities in case ParScale is not used. Implementation of simple reactions in LIGGGHTS).
- Documentation and verification against analytical solution (only possible for selected cases)
- Experimental work (setup, testing, and production experiments using a lab-scale fluidized and packed bed)
- Reversibility checks using the EL approach against results obtained with the IB.
- Validation using the EL approach against experimental results

2 Results

2.1 Verification Study

A verification study is done using a packed bed situation. Schumann [1] has provided a set of equations describing the energy conservation of associated with fluid flow through porous media (e.g., a packed particle bed), assuming a fixed fluid temperature $T_{f,in}$ at the inlet. For this problem, the analytical solution for the fluid and the particle temperatures can be written as follows:

$$\frac{T_f}{T_{ref}} = 1 - exp\left(-y-z\right)\sum_{n=1}^{\infty} y^n M_n\left(yz\right) \tag{0.1}$$

$$\frac{T_p}{T_{ref}} = 1 - exp\left(-y-z\right)\sum_{n=0}^{\infty} y^n M_n\left(yz\right) \tag{0.2}$$

with:

$$\begin{aligned} M_n\left(a\right) &= \frac{d^n M_0(a)}{d\, a^n} \\ M_0\left(a\right) &= J_0\left(2i\sqrt{a}\right) = \\ &= 1 + a + \frac{a^2}{(2!)^2} + \frac{a^3}{(3!)^3} + \ldots \end{aligned} \tag{0.3}$$

Here, J_0 is a Bessel function. The functions *y* and *z* are defined in the work of Schumann [1].

Initially, the fluid outlet temperature for both solutions is in the range of the simulation without intra-particle heat gradient. For longer run times, a lower heat flux – and thus a higher fluid outlet temperature – is predicted. Nevertheless, both – the model and the analytical solution – fit to the simulations very well and thus, can be used to quickly determine the main parameters (e.g., the required time) needed for the simulations.

Selected results for the verification study are summarized in Figure 2. Note, the Schumann solution is only valid for situations in which intra-particle heat transfer is infinitely fast. Thus, in the simulations involving ParScale, we also considered very high intra-particle heat transport rates, such that we expect ParScale-based and non-ParScale-based simulations to match. We note that the ParScale software (and hence the effect of intra-particle heat conduction) was already verified in previous studies.

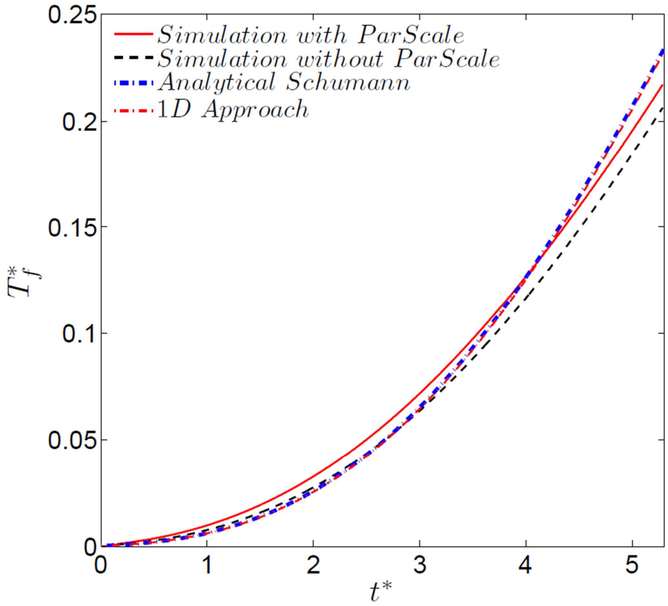

Figure 2: Comparison of the fluid outlet temperature in a packed bed.

After verifying our simulation using a packed bed operating point we can now compare it to experiments in a two-dimensional lab-scale fluidized and packed bed.

2.2 Experiments using a Lab-Scale Fluidized and Packed Bed

A semi two-dimensional particle bed is set up in which experiments of wide ranges regarding flow rate, particle mass loading and operating points can be performed. A calibrated flow meter, which is able to supply a volumetric flow (of air) up to 900 nl/min, is used to ensure fluidization of a wide range of particles. Before the air is entering the particle bed, the user can activate a heat exchanger which is designed to heat of the incoming air to over 100°C. The flow through the heat exchanger can be short-circuited via 3-way valve. To perform thermal measurements, a thermal insulation is placed inside the bed in order to minimize thermal losses to the environment. This insulation can easily be removed in case the user wants to observe the granular behavior (e.g. perform an optical measurement). The two experimental configurations are now described in detail and a real picture of the experimental set-up (thermal measurement set-up) is shown in Figure 3. In addition Figure 4 shows a schematic piping and instrumentation diagram (P&ID).

Table 2: Overview of validation experiments in the packed and fluidized bed.

Velocity (% of max. flow meter velocity)	***Material (Size)***	***Thermal Measurements***	***Optical Measurements (PIV and particle distribution)***
15;20;25;30;35	Wood (8 mm)	X	
12;18;20;24;40	Polystyrol (3-6mm)	X	
12;18;20;24;40	Glass (1 mm)		X

heat exchanger

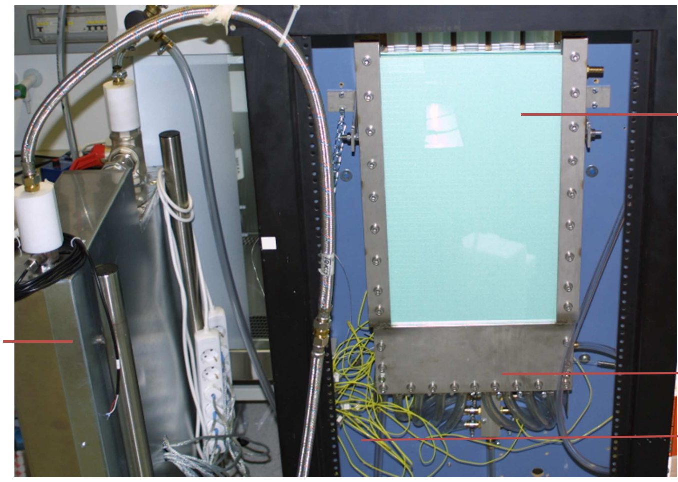

insulated wall of the particle bed

pre-mixing chamber

thermocouples

Figure 3: Set up for thermal measurement including isolated walls.

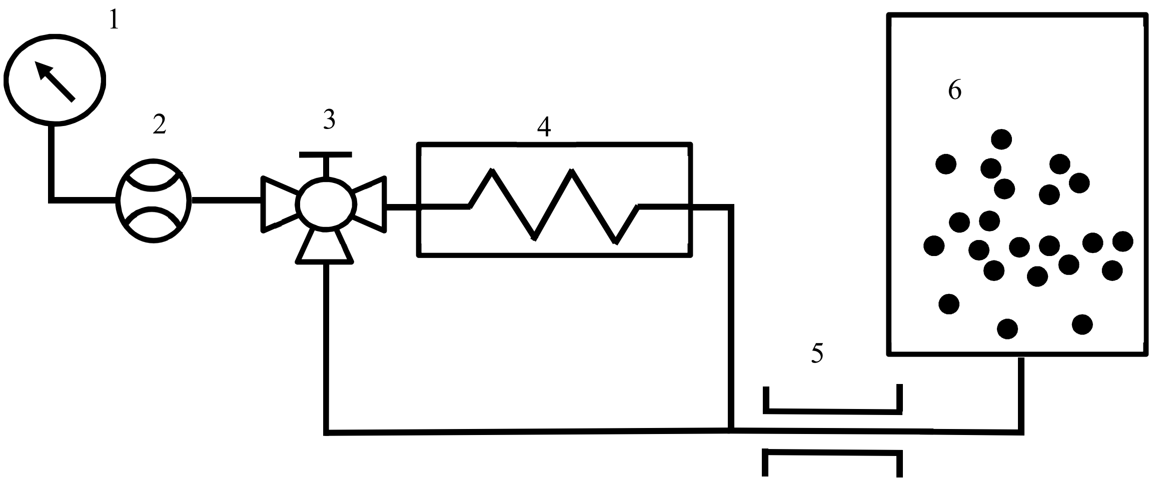

Figure 4: Schematic PID of the experimental setup (1 - pressure air supply, 2 - flow meter, 3 - three-way valve, 4 - heat exchanger, 5 - pre-mixing chamber, 6 - particle bed).

2.2.1 Optical Measurements

In order to study the particle behavior at different fluid flow rates we place a high speed camera in normal direction to the bed window. A schematic is shown in the following picture:

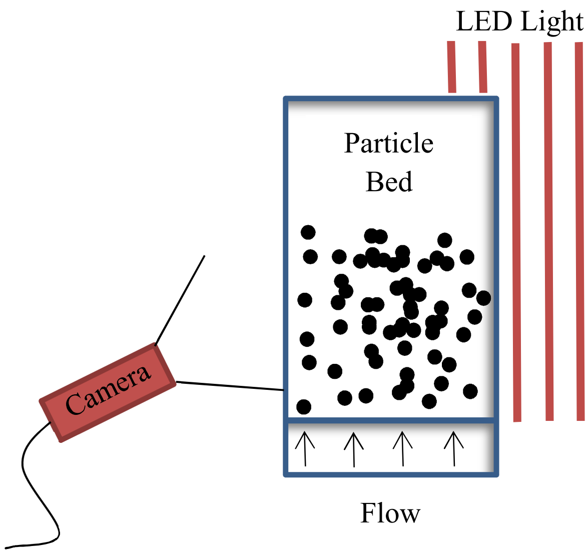

Figure 5: Schematic overview of optical measurement set-up (back light was used for better results regarding particle distribution).

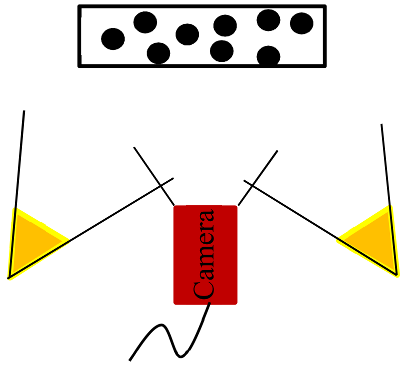

Figure 6: Schematic overview of the optical set-up used for PIV measurements (yellow triangles indicate the LED light source).

The camera can resolve the flow with up to 5,000 fps which enables us to correlate even fast particle movements. The LED light is placed in front of the bed in case granular Particle Image Velocity (gPIV) measurements are performed. The light is placed behind the fluidized bed in case the volume fraction distribution and the bubbling behavior is observed. Before the picture acquisition is started, the flow is given a sufficient time to develop within the particle bed. When choosing the camera settings, the user has to ensure that all occurring phenomena inside the particle bed can be resolved (e.g., the camera shutter time is small enough). By using post-processing routines the user can now cross-correlate all pictures, use different filters and extract average and instantaneous flow information. An example pair of picture used for cross-correlation is shown in Figure 7.

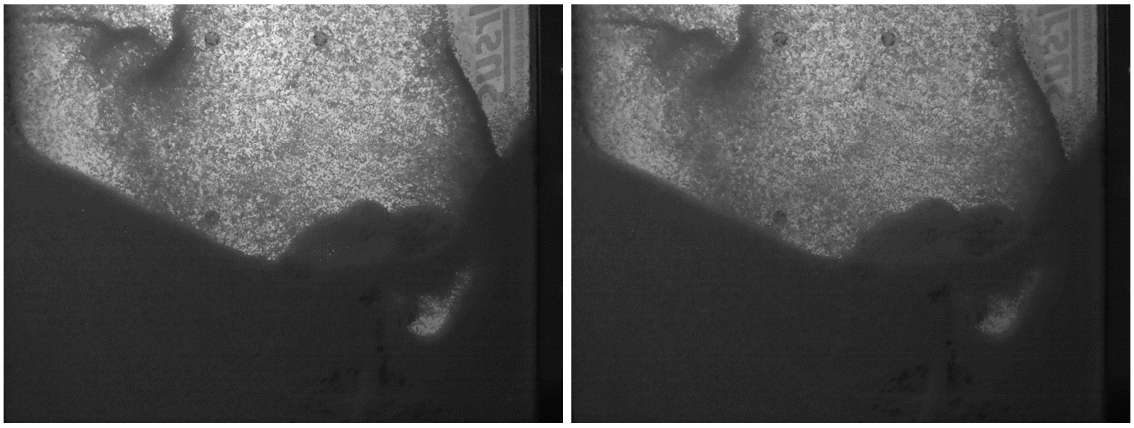

Figure 7: Pair of taken pictures used for cross-correlation (f = 500 Hz).

During cross- correlating the images, the user has the option to obtain run-time information and automatically generated flow-fields from the program (see Figure 8).

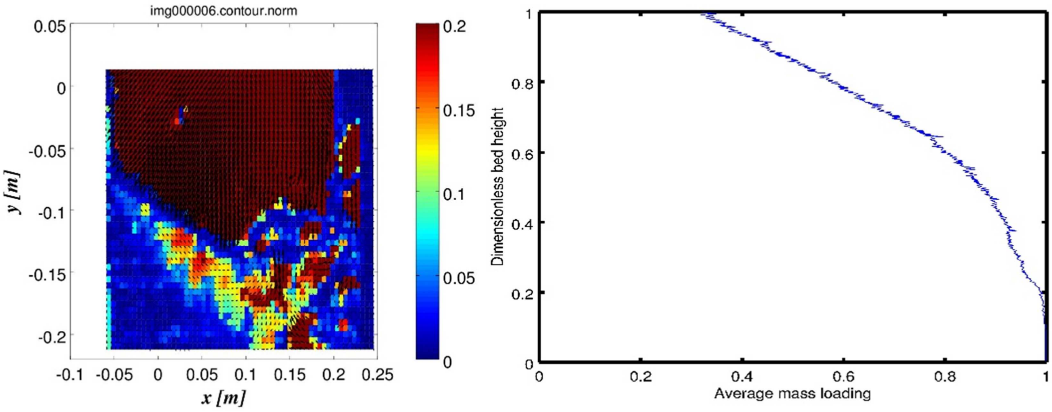

Figure 8: Results of PIV analysis (left), and averaged particle volume fraction for the dimensionless bed height (right).

For post-processing the particle movement, the user has to make sure that the captured sequence is a meaningful representation of the flow situation and occurring phenomena are depictured (e.g. cluster formation/break-up, bubble rising).

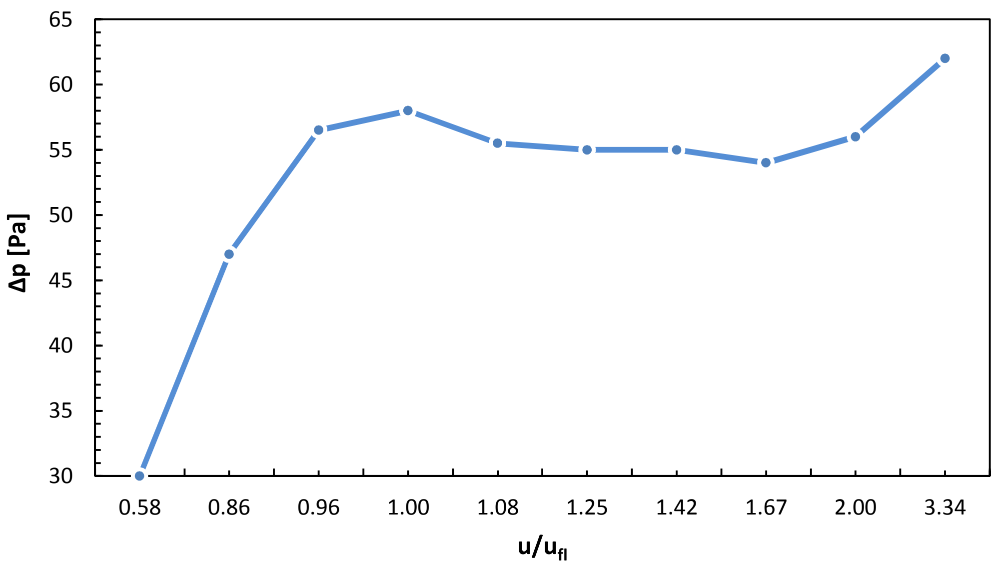

Figure 9: Typical fluidization curve of 1mm glass particles in bed (the pressure difference is plotted against the dimensionless superficial fluidization velocity).

2.2.2 Thermal Measurements

As mentioned before, the particle bed was modified to ensure correct temperature measurements. Due to the newly installed heat exchanger, the user can adjust the temperature inside the bed and perform thermal measurements up to over 100°C. Since a good insulation of the bed is the key for accurate results, a thermal insulation is placed inside the front and back window of the experimental setup. This is necessary to minimize any heat losses to the surroundings over the large window surface. Also, we placed 13 temperature probes across the back window in order to determine the temperature distribution inside the bed. An image of the temperature probes, including the insulation material is shown in Figure 10. Due to their widespread use, we use Type-K thermo-couples. Thereby, is it obvious that its thermal response time of a thermo couple is mainly a function of the diameter of the probe. Since we are limited by the thermal fitting (see Figure 11) we chose the thermo-couple diameter to be 1 mm which we experienced to be not limiting in the thermal data acquisition in any way. For connecting the thermos-couples with the computer we use a "CompactDAQ" system by National Instruments in combination with the 16 channel isothermal thermocouple input module "NI 9214". For the data acquisition program we chose "LabView" due to its flexibility and available modules fur the input module. A snapshot of the graphical interface of the measurement system can be found in Figure 12.

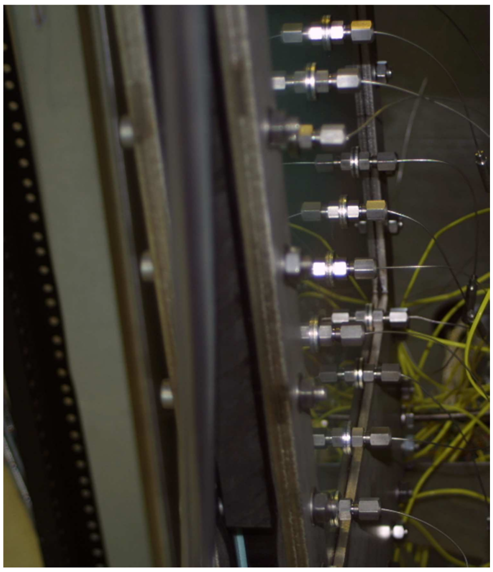

Figure 10: Thermocouples in the back plate of particle bed used for thermal data acquisition.

Figure 11: Thermo-couple fitting with minimum fitting diameter of 1 mm.

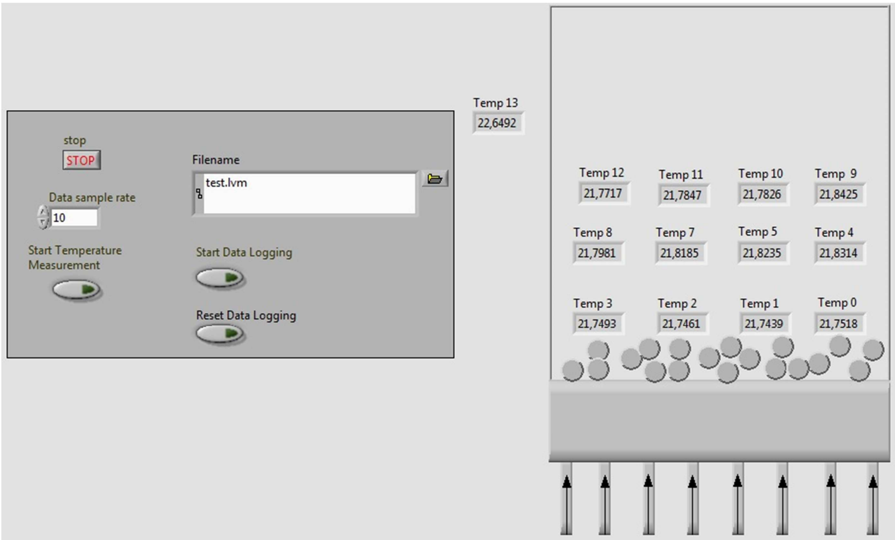

Figure 12: Screenshot of the graphical user interface, including measurement control settings (Stat/Stop, Data Logging, Sample Rate) on the left side and temperature sensor values on the right side.

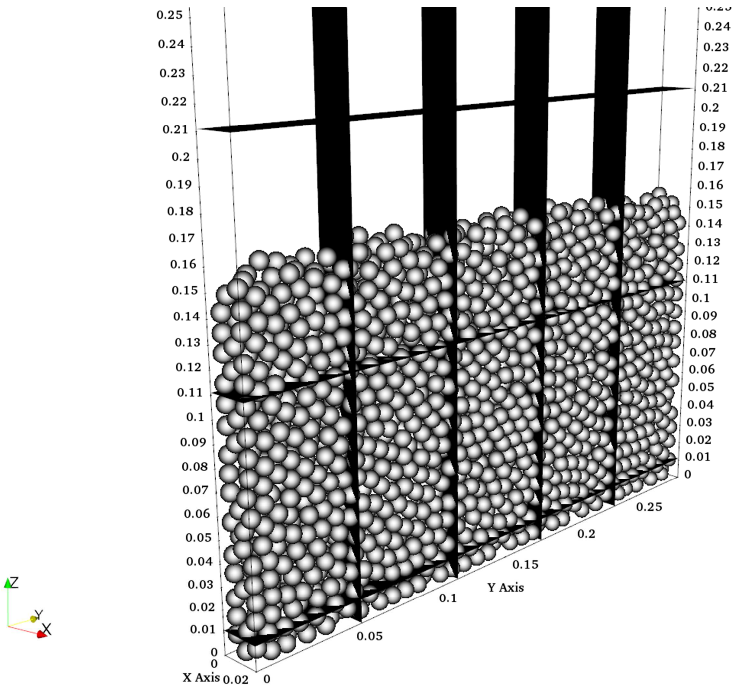

Figure 13: Positioning of thermocouples at the interface of the slices (x-position [0.01], y – positions: [0.57 0.117 0.177 0.237], z-positions: [0.011 0.111 0.211]).

2.3 Verification and Validation Study for Fluidized and Packed Bed

We perform a full-scale simulation of the packed bed described in the previous chapter in order to provide a 1:1 validation of our simulation tool. Even though we collected data for several parameter setups, we now focus only a single validation case for the configuration specified in Table 3. This case is most challenging, since used particles have a significant intra-particle resistance to heat conduction, which necessitates the use of an adequate simulation model (i.e., ParScale coupled to CFDEM®).

Table 3: Simulation parameters for the validation case.

PROPERTY	VALUE
particle count	2,000
particle size (wood)	8 [mm]
particle density (wood)	750 [kg/m³]
particle heat capacity (wood)	2,000 [J/kg K]
particle heat capacity (wood)	0.16 [W/m K]
inlet velocity	1.18 [m/s]

For the thermal validation, we make use of the coupling between CFDEM® and ParScale (i.e., we use the COSI platform) to correctly account for internal temperature profiles inside of each particle. The particles are initialized according to the initial temperature measured from the experiment (this is done to avoid the simulation of the initial heat up phase). An automatic routine is set up to place the particles in boxes and initialize them with the temperature measured in that region. An illustrate of such an automatic particle and particle temperature generation is shown in Figure 14.

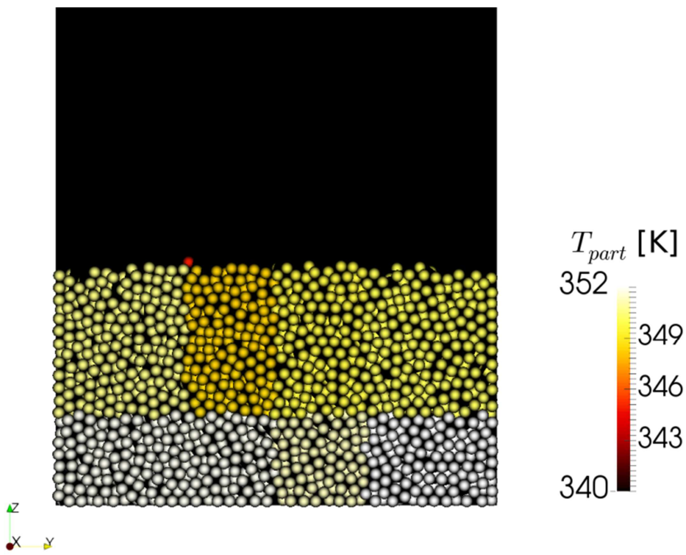

Figure 14: Initial particle configuration including region depending temperature.

Also, the inlet temperature is measured and used as a time dependent input parameter in the simulation. This is important since the system shows different cooling behavior at different flow rates (due to the thermal inertia of the piping and distributors in the experiment). We run reach validation simulation for 60 seconds real time which provides a sufficient amount of information on the cooling process of the packed bed. After the simulation, automatic post processing routines provide a wide range of temperature plotting options. Figure 15 pictures an example from a finished simulation including particle temperatures and corresponding fluid temperature field.

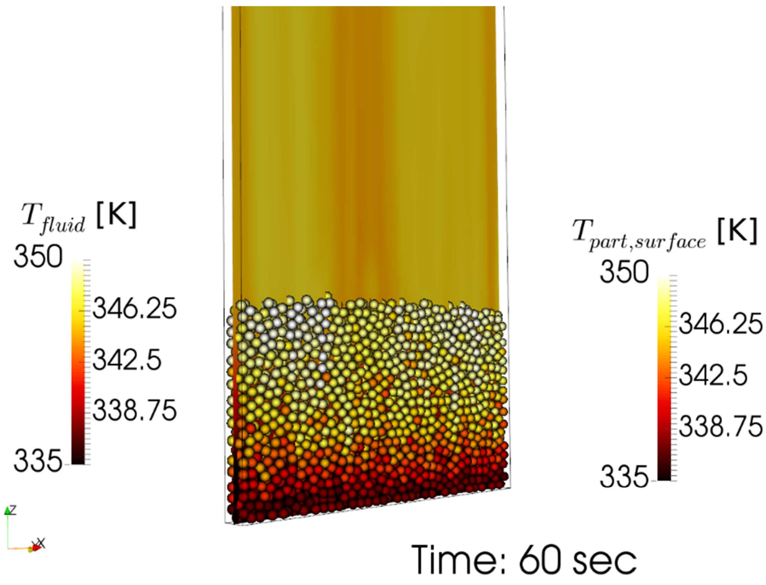

Figure 15: Temperature distribution at the quasi steady-state of a CFDEM® simulation.

For a thermal validation we pick average fluid temperatures in the horizontal direction (see Figure 16, H1/H3) and compare the mean temperature in thse layers in Figure 17.

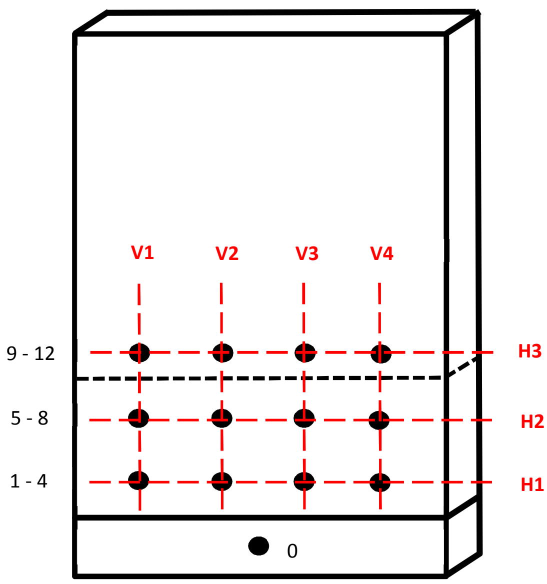

Figure 16: Temperature measurements including vertical and horizontal averaging for post-processing. Black numbers indicate thermocouple numbering, red numbers indicate averaging labels.

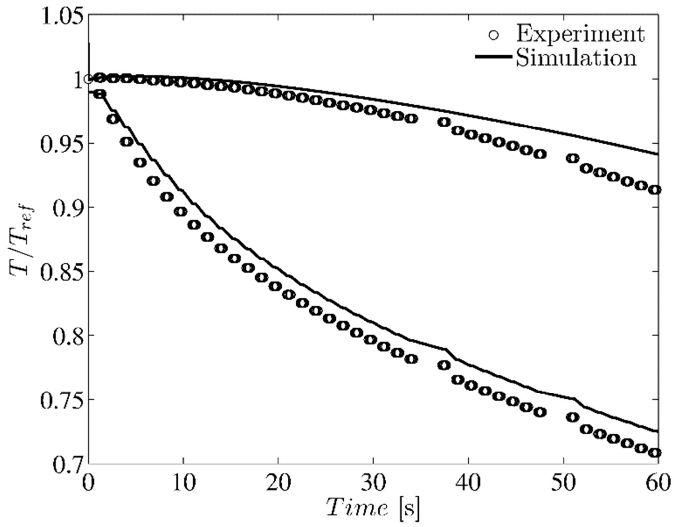

Figure 17: Horizontal mean fluid temperatures for layer H1 (bottom line and symbols) and H3 (top line and symbols, compare Figure 8).

Generally, a good agreement between experiment and simulation can be observed. The thermal inertia of the particle bed can be seen, especially in the H3 layer (top line and symbols in Figure 17). This behavior is also visible from Figure 15, where the particle temperature is still close to the initial temperature. The occurring differences are mainly due to the following limitations of the current simulation model:

- Adiabatic, isothermal walls in the simulation (i.e., we do not account for heat losses to the environment)
- Dispersion due to pseudo-turbulent gas flow is not accounted for in the simulation model
- The heat transfer correlation (currently, we used the Gunn correlation) might be inaccurate
- Flow inlet profil is unknown – the simulation considers a block profile
- Uncertaincy in the particle properties
- Temperature independent particle and fluid properties in the simulation (integral values were used)

A good, but less excellent agreement is also found when comparing vertical averaged temperatures (e.g. V2, V3; see Figure 18). It is speculated that differences are again due to the above mentioned limitations.

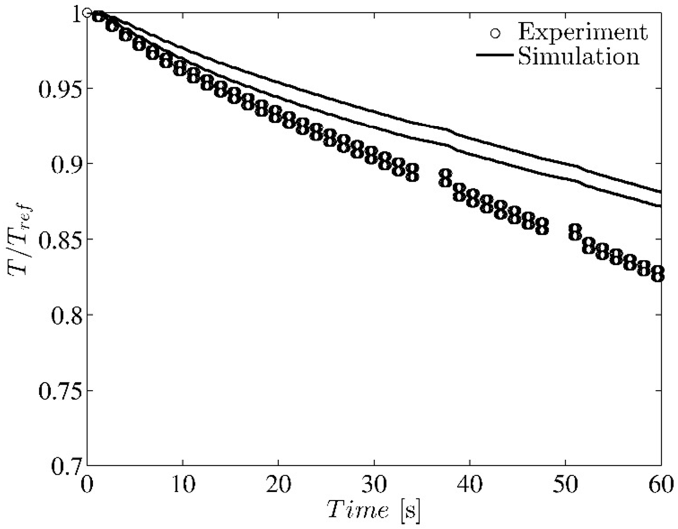

Figure 18: Validation of vertical averaged temperatures over time (upper graph: V2, lower graph: V3).

2.4 Reversibility Checks

In order to check our simulations towards reversibility, we perform Direct Numerical Simulation (DNS) using the novel HFD-IB (Hybrid Fictitious-Domain/Immersed-Boundary) method and we compare to unresolved Euler-Lagrange (EL) simulations. To draw a meaningful comparison we initialize both simulations with the same set of particle positions and set all dimensionless quantities to be equal. Here, cold air is entering the simulation domain and is heated up by the thermal energy release of the particles. Due to the relative high Reynolds number (and consequently the high Peclet number) we do not observe significant temperature saturation in the particle bed. The simulation set-up and domain is kept the same, but clearly a much higher resolution, in terms of both grid size and time step, is required for DNS compared to unresolved Euler-Lagrange simulations.

Table 4: Parameters used in the comparison between DNS and EL simulations.

Simulation parameter	***Value***
Simulation domain (x y z)	10 x 2.5 x 20 $\boldsymbol{d_p}$
Particle diameter $\boldsymbol{d_p}$	1 [*dimensionless*]
Reynolds number $\boldsymbol{Re}$	600
Prandlt number $\boldsymbol{Pr}$	1
Number of cells (EL) (x y z)	10 x 6 x 20
Number of cells (DNS) (x y z)	250 x 63 x 500
Particle resolution in DNS $\boldsymbol{\frac{d_p}{\Delta x}}$	25
Number of particles	300
Nusselt number correlation (EL)	Gunn
Dimensionless time step $\boldsymbol{\Delta\tau = t\frac{U_{in}}{d_p}}$	10^{-4}

In order to compare the two methods, the average fluid temperature (i.e., the “cup-mixing temperature) is calculated at several positions in the bed (see the slices depicted in Figure 19). The flux-weighted average fluid temperature can be expressed as:

$$\tilde{T}\big|_S = \frac{\int_S \phi u_f T dS}{\int_S \phi u_f dS}$$

Being S the sampling surface and (ϕu_f) the volumetric fluid flux interpolated at S.

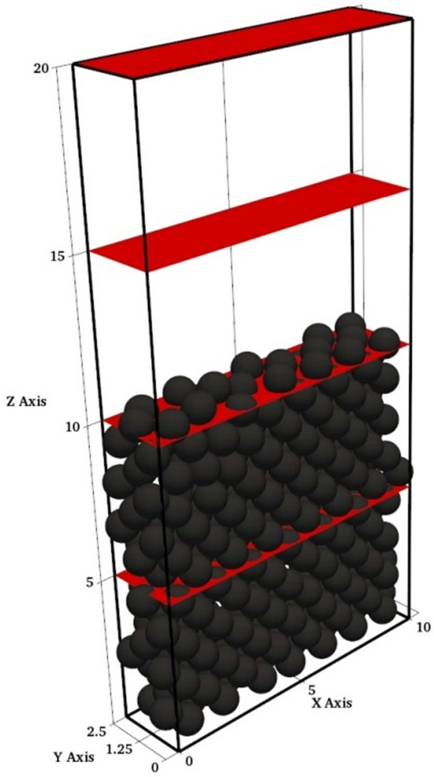

Figure 19: Fluid domain and particle configuration for the DNS and PU-EL simulations. Average fluid temperature is calculated for each red slice. The bottom XY plane is set with an inflow boundary condition while the top XY plane with an outflow boundary condition. YZ planes are periodic surfaces and XZ planes are walls.

2.4.1 Results of Particle Unresolved Euler-Lagrange (PU-EL) Simulations

From the PU-EL simulations per-particle Nusselt numbers and temperature profiles were analyzed, for which results are shown in Figure 20, as well as Figure 21. As can be seen, there is little variation with respect to the laterial position, however, the Nusselt numbers drop significantly (and systematically) near towards the boundaries of the bed in the flow direction. This is mainly due to the smearing out of the voidfraction field in these regions, which drastically affects the Nusselt number.

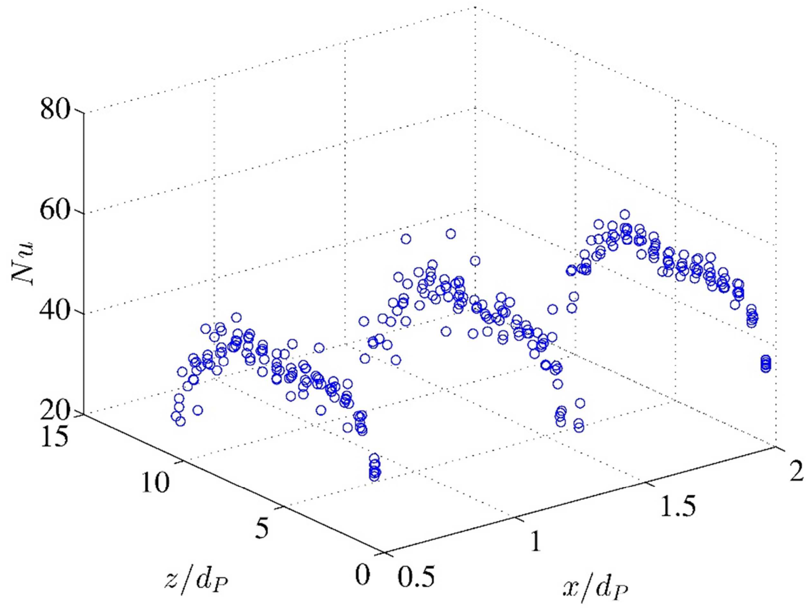

Figure 20: Per-particle Nusselt number as a function of the lateral position (x), as well as the position in the flow direction (i.e., the height z).

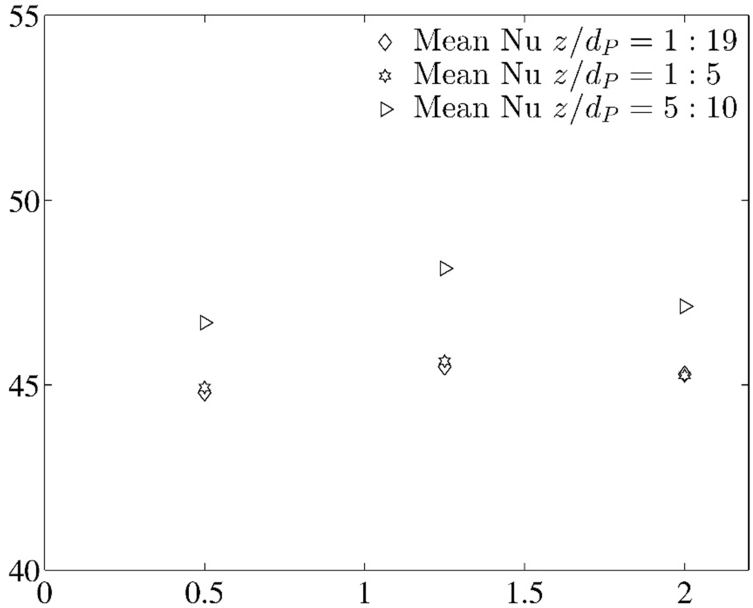

Figure 21: Mean Nusselt number as a function of the lateral position (x) for different averaging intervals in the flow direction (i.e., the height z).

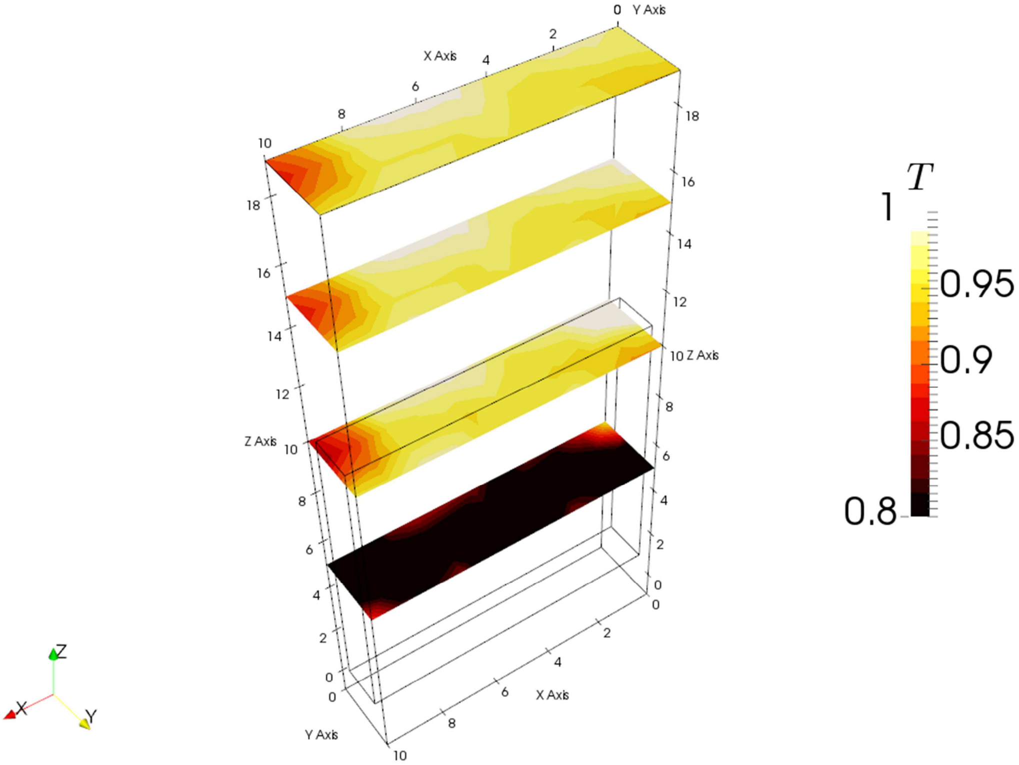

Figure 22: Slices used for comparing the average temperature at different bed heights (results are compared to predictions based on DNS in Chapter 2.4.2). The small black box demarcates the particle filling inside the simulation region.

Figure 22 and Figure 23 show results for the fluid velocity and temperature distribution, illustrating a fast heat up of the fluid in the bed, and litle lateral temperature gradients.

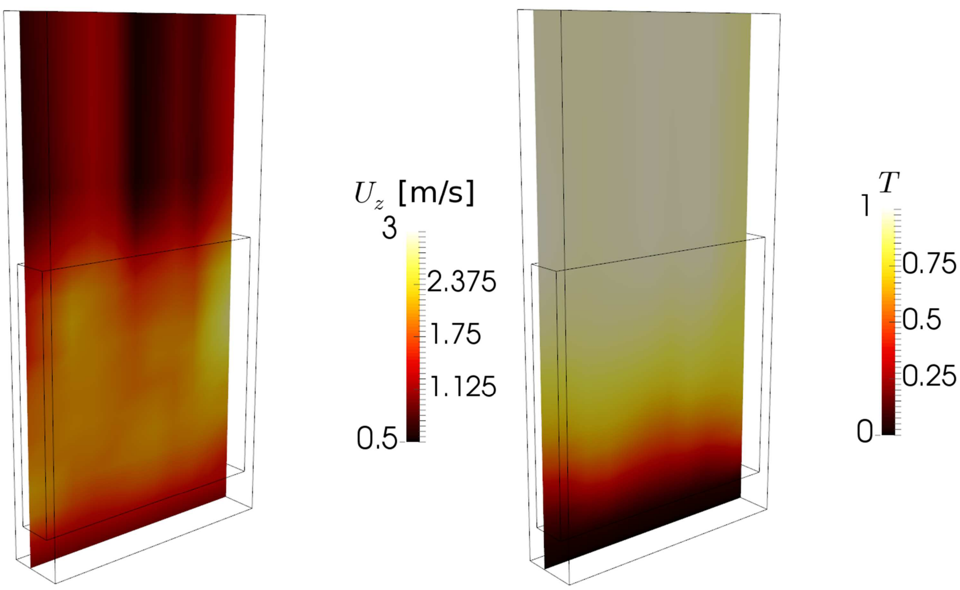

Figure 23: Snapshot of the fluid flow field from the particle-unresolved EL simulations (PU-EL) used for the reversibility checks (left). The right panel shows the temperature distribution in the fixed bed for the PU-EL simulation.

2.4.2 Results of Direct Numerical Simulations

Figure 24 shows the dimensionless temperature field in the fixed bed at different time steps for the DNS. These simulatoins typically take up ~ 15,000 CPUhrs, and are hence rather expensive. We notice that the HFD-IB method is able to trigger small-scale structures in the simulated fields, as one would expect from particle-resolved simulations. In contrast to previous work that mainly relied on body-fitted meshes, the HFD-IB allows to retain the full description of all flow details, while using a simple structured grid to perform the computation. Thus, no tedious meshing is necessary, and also moving particles can be handled with ease.

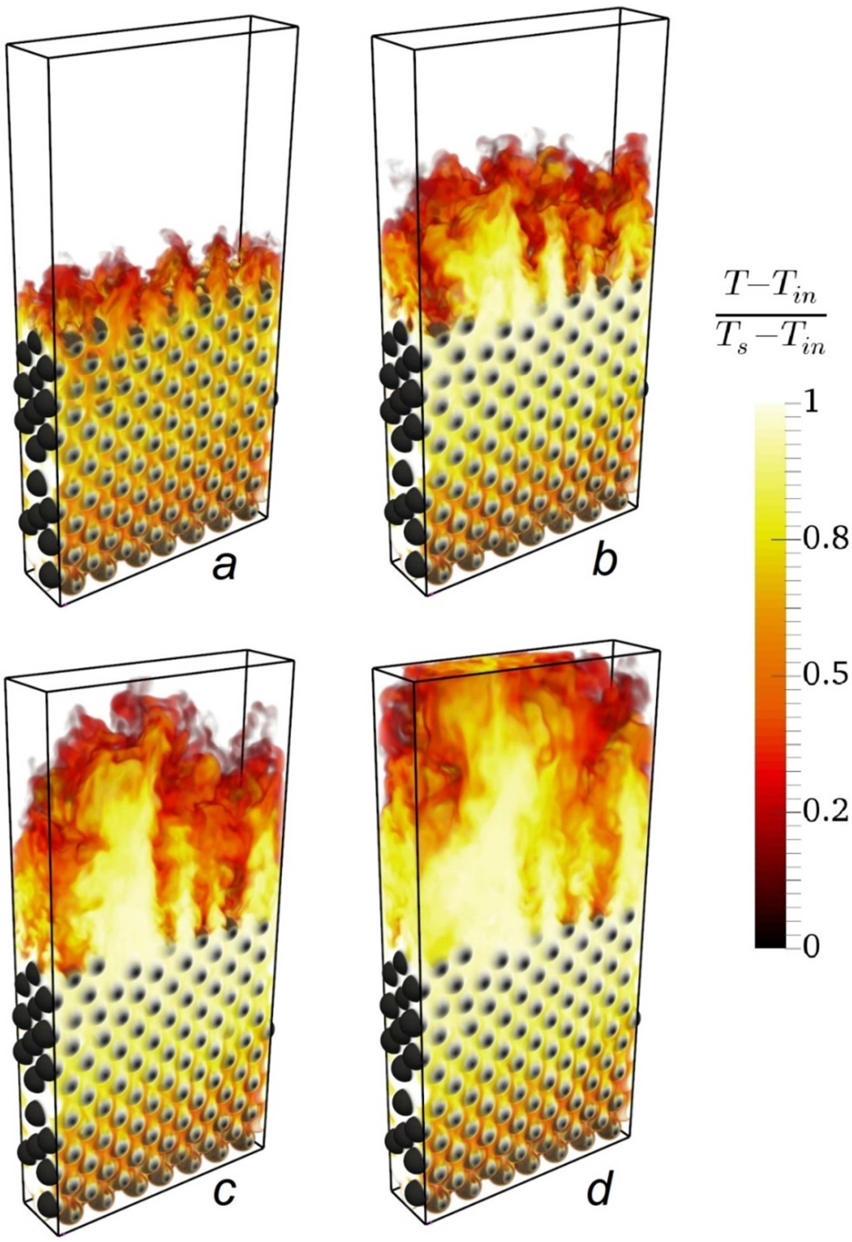

Figure 24 : Volume rendering of the dimensionless temperature field at different dimensionless times $\tau = \frac{d_p}{U_{in}}$ (a: $\tau = 1$, b: $\tau = 3$, c: $\tau = 5$, d: $\tau = 8$). Particles are colored in dark grey and periodic particles are not mirrored (i.e., they are represented only on one side).

Figure 25 compares the slice-averaged (flux-weighted) temperatures between the DNS and the PU-EL simulations. As can be seen, two key differences are observed: (i) the DNS data predicts higher fluid temperatures, i.e., a faster heat transfer than the PU-EL. This is mainly due to wall effects discussed in the next paragraph. (ii) The temperature response predicted by the DNS is one to two dimensionless time units faster compared to the PU-EL. It is speculated that this is due to the fact that the PU-EL currently does not account for spatial dispersion (which, unfortunately, could not be implemented due to a missing model).

Figure 26 reveals the more important finding from our DNS that particles close to the wall experience a much higher Nusselt number compared to that near the center of the bed. Physically this enhanced heat transfer is caused by wall effects that lead to very high fluid velocities near the wall (data not shown). A comparison with currently available closures (i.e., that of Gunn and Deen et al.) indicates that this effect is massive, and results in mispredictions of up to ca. 300%. Fortunately, it appears that this effect is just observed for particles touching the wall, since Nusselt numbers for particles more distant from the wall agree well with currently available closure models.

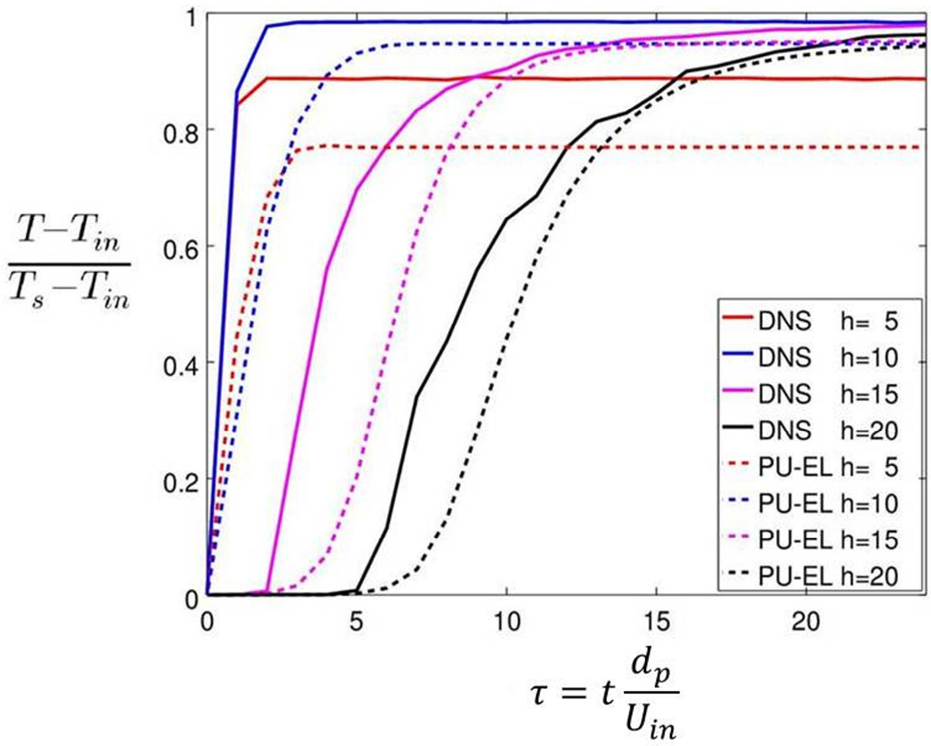

Figure 25: Time evolution of the dimensionless averaged temperature evaluated at the sampling slices shown in Figure 22. The temperature field in the particle bed reaches the pseudo-stationary state around and $\tau \approx 2$ in the DNS and $\tau \approx 5$ in the PU-EL. Notice that in the wake region, the average temperature increases up to the maximum average temperature inside the bed.

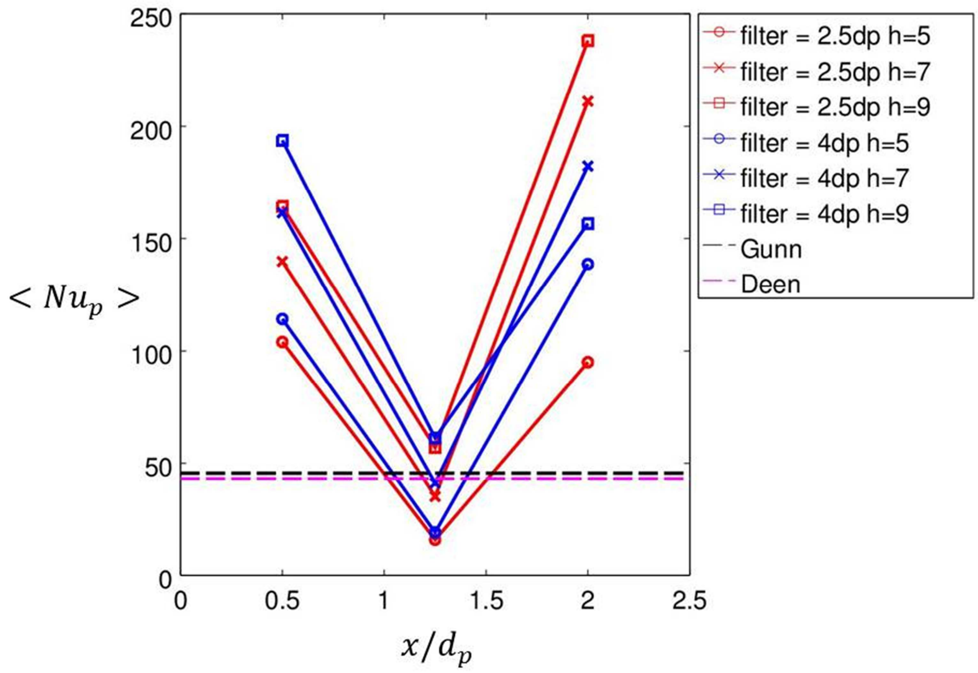

Figure 26: Spatially-averaged particle based Nusselt number as a function of the wall distance and the bed height. Near the walls values are considerably higher than what Gunn's or Deen et al.'s correlation would predict.

2.5 Demonstration Cases: Fluidized and Packed Beds with and without Reactions

An array of simulations to illustrate effects of intra-particle diffusion effects was performed for packed and fluidized beds. Selected results of such simulations (utilizing the full COSI platform, i.e., a co-simulation involving LIGGGHTS®, CFDEM® and ParScale) are summarized in Figure 27. Typical simulation times for a typical simulation ($25 \cdot 10^3$ particles, discretized with 10 intra-particle grid points each) are in the order of one CPU·day.

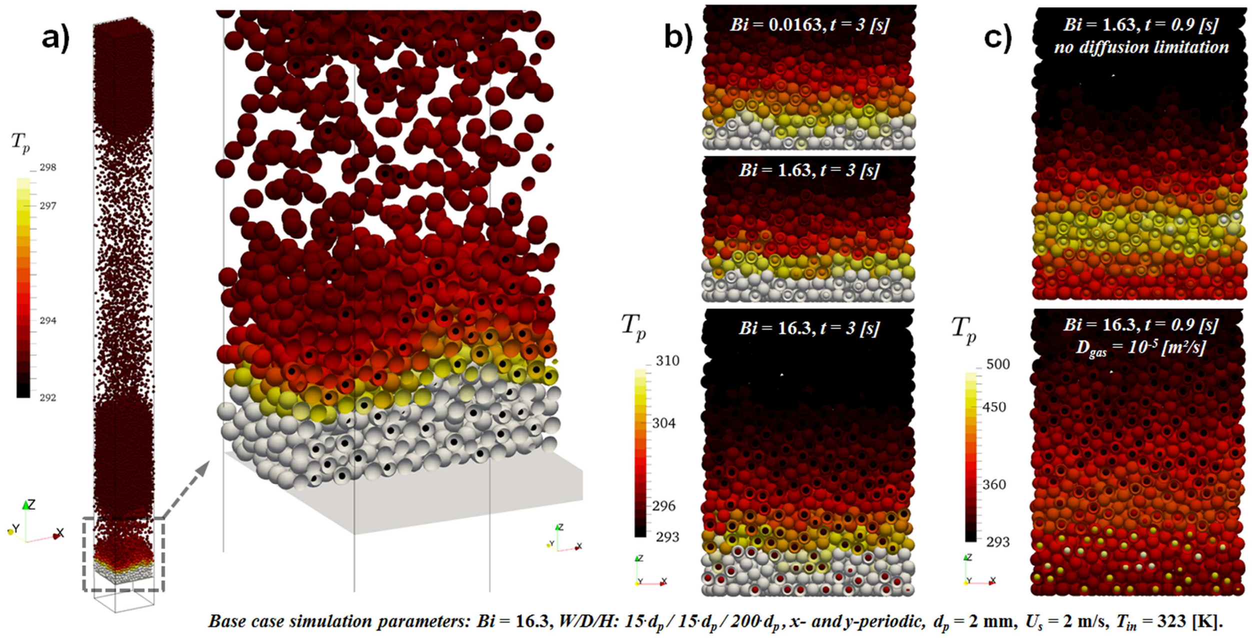

Figure 27 : Temperature distribution in a fluidized, and a packed bed setup (25,000 particles, each particle is discretized using 10 radial points; a: fluidized bed with close-up view near the inlet, b: packed bed, c: reactive packed bed).

In order to illustrate a typical application of the unresolved CFDEM® approach with reactions, a two-zone fluidized bed reactor (i.e., an FB reactor with two gas injection ports) was simulated (see Figure 28; these simulations were done without coupling to ParScale, since gas concentration gradients will be small). For the considered system ($250 \cdot 10^3$ particles, particle diameter 140 [µm], 1.4 [cm] bed width, 7 [s] simulated time), running on 4 standard XEON CPUs, a simulation time of 38 [hrs] was required.

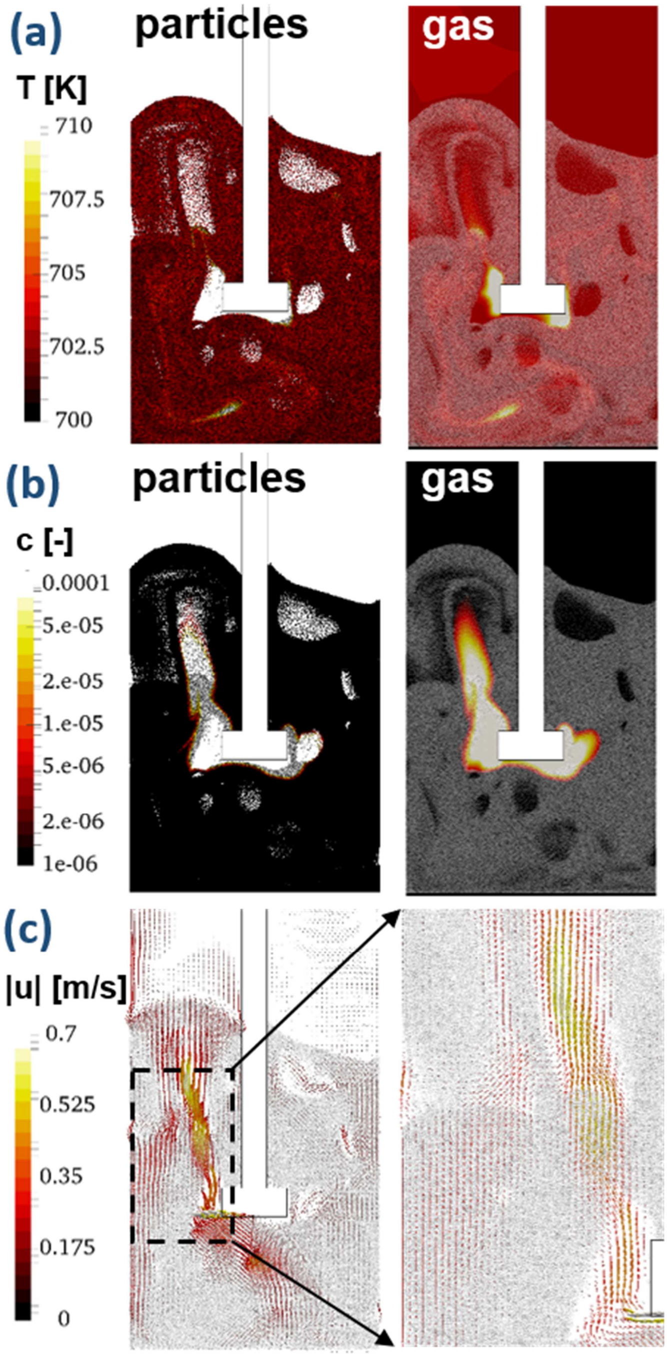

Figure 28 : Instantaneous temperature (a), educt concentration (b), and gas flow field (c) in explorative fully-physics simulations of a TZFBR (fast chemical reaction; video available at http://goo.gl/HXB5xm).

3 Conclusion

The results of (i) experiments, (ii) very detailed Direct Numerical Simulations, as well as (iii) unresolved CFD-DEM simulations were critically compared. This was done to (i) demonstrate the functionality of NanoSim's open-source co-simulation platform, and (ii) to identify shortcomings of currently available models. Some fundamental insight was gained, mainly related to the difficulties to model heat transfer rates (to particles) in the vicinity of walls. It is now clear that available models in literature cannot accurately predict the heat transfer rate from particles touching the wall. Also, dispersion of thermal energy appears to be substantial, requiring additional closures to refine our predictions of unresolved EL simulations in future.

Finally, it has to be mentioned that while the comparison against experimental data was largely successfully, the experiments still suffer from the inability to substantiate the amount of heat lost to the environment. While this heat loss is not of critical importance for industrial applications (due to the larger dimensions of these systems), future experimental work may focus on an even more complete suppression of unwanted heat losses.

4 Appendix

4.1 Glossary

See List of definitions and abbreviations in Section 1.3

4.2 Document Change Log

Date	Description	Author(s)	Comments
30.05.2016	Preliminary version (0.1)	S. Radl	Outline
30.06.2016	First draft (1.0)	T. Forgber	
04.07.2016	Update (1.1)	S. Radl	
20.07.2016	Update (1.2)	T. Forgber, F. Municchi, S. Radl	Final update and check

5 References

[1] T.E.W. Schumann, Heat transfer: A liquid flowing through a porous prism, J. Franklin Inst. 208 (1929) 405–416.